

# On the use of multivariate autoregressive models for vibration-based damage detection and localization

Alessandra Achilli<sup>1</sup>, Giacomo Bernagozzi<sup>\*1</sup>, Raimondo Betti<sup>2</sup>,  
Pier Paolo Diotallevi<sup>1</sup>, Luca Landi<sup>1</sup>, Said Quqa<sup>1</sup> and Eleonora M. Tronci<sup>2</sup>

<sup>1</sup> Department DICAM, University of Bologna, Bologna, Italy

<sup>2</sup> Department of Civil Engineering and Engineering Mechanics, Columbia University, New York, USA

(Received July 7, 2020, Revised September 9, 2020, Accepted October 3, 2020)

**Abstract.** This paper proposes a novel method suitable for vibration-based damage identification of civil structures and infrastructures under ambient excitation. The damage-sensitive feature employed in the presented algorithm consists of a vector of multivariate autoregressive parameters estimated from the vibration responses collected at different locations of the analyzed structure. Outlier analysis and statistical pattern recognition are exploited for damage detection and localization. In particular, the Mahalanobis distance between a set of reference (i.e., “healthy”) and inspection parameters is evaluated. A threshold is then selected to determine whether the inspection vectors refer to damaged or undamaged conditions. The effectiveness of the proposed approach is proved using numerical simulations and experimental data from a benchmark test. The analysis results show that the largest values of Mahalanobis distance can be found in the proximity of those sensors closest to the damaged elements. Thus, the Mahalanobis distance applied to vectors of multivariate autoregressive parameters has proven to be a robust indicator for damage detection and localization.

**Keywords:** structural health monitoring; damage detection; multivariate autoregressive model; outlier analysis; Mahalanobis distance

## 1. Introduction

Output-only techniques in vibration-based Structural Health Monitoring (SHM) are rapidly emerging as an effective tool to assess the condition (e.g., “health”) of structures, especially in recent years, since a growing number of structures and infrastructures are approaching their service life. Excellent overviews in this topic can be found in (Das *et al.* 2016, Fan and Qiao 2011, Farrar and Worden 2007, Sohn *et al.* 2004). Modal parameters have been largely used as damage-sensitive features (DSFs) due to their direct physical interpretation. In particular, modal shapes have been shown effective in damage localization, even though they are not as sensitive to small damage (Farrar and Worden 2013). Other techniques involving pattern recognition and outlier analysis have recently gained attention and are becoming more popular in SHM applications (Farrar and Worden 2013, Worden *et al.* 2000).

In this context, AutoRegressive (AR) models have been extensively used in the description of dynamic systems, mainly thanks to their low computational complexity (Ljung 1987, Guidorzi 2003). Several studies have been conducted in the civil engineering field to identify dynamic systems using AR models and related extensions (Guidorzi *et al.* 2014, Brincker and Ventura 2015), to find a synthetic

representation of the complex structural behavior or retrieve modal features. Univariate AutoRegressive (UAR) models, i.e., models that consider recorded signals individually, have been largely employed for damage identification, typically using novelty detection techniques that generate control charts. However, evaluating a damage index based on localized recordings may be misleading if the signal is collected in parts of the structure that are not representative of the overall dynamic behavior (e.g., at locations in the proximity of modal shape nodes).

Nair *et al.* (2006) proposed a DSF based on multiple sets of parameters identified assuming a univariate AR model per recording channel. In this case, however, the inherent relation among different channels is neglected. Recently, some techniques have been proposed to take into account spatial information employing the parameters of Multivariate AutoRegressive (MAR), also addressed as ‘vector’, models. Such methods generally lead to a more robust damage indicator, as shown by Goi and Kim (2017). Wang and Ong (2008) proposed using Hotelling’s  $T^2$  control chart to monitor the coefficients of a multivariate AR model fitted to acceleration responses collected at multiple locations of a structure. This method enables more robust damage detection for large structures than univariate approaches.

Initial investigations on damage localization using multivariate AR models were conducted by Heyns (1997), De Stefano *et al.* (1997), Bodeaux and Golival (2003), who retrieved natural frequencies and modal shapes from Vector Autoregressive Moving Average (VARMA) models.

\*Corresponding author, Ph.D.,  
E-mail: [giacomo.bernagozzi2@unibo.it](mailto:giacomo.bernagozzi2@unibo.it)

Mosavi *et al.* (2012) employed the first two elements on the main diagonal of the matrices of AR parameters relevant to the two most recent time lags as a DSF that also include spatial information. In particular, a study on the variation of this indicator was evaluated between a baseline and a set of inspection signals. More recently, Roy *et al.* (2015) showed a direct relationship between the coefficients of a multivariate AutoRegressive with eXogenous input (ARX) model and the normalized structural stiffness. In the mentioned work, ARX parameters are used for precise damage localization by defining a damage index at all the Degrees of Freedom (DOFs) except one, which is assumed as the location where excitation is applied. This model makes, therefore, necessary repetition of the identification process, assuming a different response channel at a time as exciting input to evaluate damage at all instrumented locations. Also, the application of this method to structures where excitation can be modeled as uncorrelated white noise at each DOF is challenging.

AR models have great potential in data-based SHM applications due to their simple structure and sensitivity to damage in comparison with modal-based approaches. However, in this context, few studies have been conducted for localizing damage in civil structures. In this paper, a novel approach for damage detection and localization is presented, based on outlier analysis performed using the parameters of a MAR model identified by means of structural vibration responses. Contrary to most AR-based literature methods, such as the ones presented in Mosavi *et al.* (2012) and Loh *et al.* (2016), the main novelty of the proposed approach consists of exploiting all the parameters of the selected MAR model to retrieve accurate spatial information about the structural state of health. The damage index is indeed represented in a two-dimensional map whose elements indicate the structural portions included among all the possible combinations of the instrumented locations.

The method proposed herein is validated using the vibration data of two benchmarks, a numerical model representing a 5-DOF frame excited at all the levels and an experimental 4-DOF steel frame with excitation applied to the lowest DOF.

## 2. From univariate to multivariate autoregressive models: an overview

An AR model is a numerical model that can be used to describe the dynamic behavior of a system and that can be identified only employing the output response of the system. AR model identification is thus performed without considering any input, and this represents the main difference with respect to the identification of ARX models (Guidorzi 2003). Due to their characteristics, AR models can be employed in the field of civil engineering for identifying the behavior of structures and infrastructures under ambient excitation, where measuring the excitation input is impractical.

In general, in the identification of AR models, the outputs of the analyzed system can be considered either individually or simultaneously, generating univariate or

multivariate models, respectively.

A univariate autoregressive model can be expressed by the following equation

$$y(k) = \sum_{i=1}^p a_i y(k-i) + e(k) \quad (1)$$

where  $y(k)$  is the output at the  $k$ -th time step (e.g., a measured time sequence), where  $k = p+1, p+2, \dots, l$ , and  $p$  is the model memory (which is equal to the model order in the univariate case). The parameter  $l$  represents the total number of samples of the considered output sequence  $y(1), y(2), \dots, y(l)$ . The autoregressive coefficients are indicated with  $a_i$  ( $i = 1, 2, \dots, p$ ) while  $e(k)$  is a stochastic white process with a null expected value. As shown in Eq. (1), the output at time  $k$  is expressed as a linear combination of  $p$  past outputs. This link between the present output and the past values is however not exact when considering the measured noisy responses of real systems. This is accounted by the introduction in the model of the error term  $e(k)$ . As shown in Guidorzi (2003), an autoregressive model expressed in the form of Eq. (1) belongs to the family of the equation error models.

Assuming that the AR coefficients of the model are known, it is possible to obtain the one-step-ahead prediction of the output starting from the measured  $p$  past outputs. This operation can be expressed in analytical form by considering a row matrix of autoregressive parameters  $\mathbf{a} = [a_p \ a_{p-1} \ \dots \ a_1]$  with dimension  $(1 \times p)$  and a Hankel matrix  $\mathbf{H}_1$ , of dimensions  $p \times (l-p)$ , formed by the past outputs

$$\mathbf{H}_1 = \begin{bmatrix} y(1) & y(2) & \dots & y(\ell-p) \\ y(2) & y(3) & \dots & y(\ell-p+1) \\ \vdots & \vdots & \dots & \vdots \\ y(p) & y(p+1) & \dots & y(\ell-1) \end{bmatrix} \quad (2)$$

The one-step-ahead prediction of the output can then be obtained as follows

$$\tilde{\mathbf{h}}_2(\mathbf{a}) = \mathbf{a} \mathbf{H}_1 \quad (3)$$

where  $\tilde{\mathbf{h}}_2(\mathbf{a}) = [\tilde{y}(p+1, \mathbf{a}) \ \tilde{y}(p+2, \mathbf{a}) \ \dots \ \tilde{y}(l, \mathbf{a})]$  is a row matrix with dimension  $1 \times (l-p)$  formed by the values of the predicted outputs associated with a set of AR coefficients  $\mathbf{a}$ . The difference between the measured outputs  $y(k)$  and the predicted outputs  $\tilde{y}(k, \mathbf{a})$  is denoted as prediction (or residual) error

$$\varepsilon(k, \mathbf{a}) = y(k) - \tilde{y}(k, \mathbf{a}) \quad (4)$$

which is evaluated for  $k = p+1, p+2, \dots, l$ . The estimation of AR coefficients is performed by minimizing a cost function, which usually has the following expression

$$J(\mathbf{a}) = \frac{1}{l-p} \sum_{k=p+1}^l \varepsilon(k, \mathbf{a})^2 \quad (5)$$

As shown in Eq. (5), the cost function is the mean of the squares of the prediction errors (also denoted as mean

square prediction error), and it coincides with the variance of the prediction errors. To minimize this cost function and estimate the AR coefficients, the Least Squares (LS) method can be employed. At first, the Hankel matrix  $\mathbf{H}_1$  and the row matrix  $\mathbf{h}_2$  are formed starting from the measured outputs. Then, the LS estimate  $\hat{\mathbf{a}}$  for the row matrix  $\mathbf{a}$  can be found as follows

$$\hat{\mathbf{a}} = \mathbf{h}_2 \mathbf{H}_1^+ \quad (6)$$

where  $\mathbf{H}_1^+$  is the pseudoinverse of the matrix  $\mathbf{H}_1$ . Eq. (6) is obtained by inverting Eq. (3), and by considering the row matrix  $\mathbf{h}_2$  of the observations in place of the row matrix  $\tilde{\mathbf{h}}_2(\mathbf{a})$  of the predictions.

When estimating the AR coefficients, the selection of the memory of the model (i.e., the model order in the univariate case) is one of the most important aspects. To this purpose, memory selection criteria can be employed, such as, the Akaike Information Criterion (AIC) (Akaike 1974), the Bayesian Information Criterion (BIC) (Schwarz 1978), the Predicted Per Cent Reconstruction Error criterion (PPCRE) (Guidorzi *et al.* 1982), and the mean square error criterion (Simani *et al.* 2003). In this selection, it is important to find a memory that guarantees a good accuracy of the model - i.e., minimizing the estimation errors, while avoiding overfitted models with a number of unnecessary parameters.

On the other hand, a multivariate autoregressive model can be defined through the following equation

$$\mathbf{y}(k) = \sum_{i=1}^p \mathbf{A}_i \mathbf{y}(k-i) + \mathbf{e}(k) \quad (7)$$

where  $\mathbf{y}(k)$  is a vector containing all the measured outputs at time step  $k$  (with dimension  $m \times 1$ ),  $\mathbf{A}_i$  is the autoregressive matrix that contains the AR parameters (with dimension  $m \times m$ ),  $\mathbf{e}(k)$  is the  $m \times 1$  vector of the equation error (the components of which are stochastic white processes with null expected value), with  $m$  being the number of the time histories considered in the analysis (e.g., the number of the recorded vibration responses of a structural system, measured at different locations). As already defined for the univariate case,  $p$  is the model memory, and  $k = p+1, p+2, \dots, l$ , where  $l$  represents the total number of samples of the considered output sequence  $y_j(1), y_j(2), \dots, y_j(l)$ , with  $j = 1 \dots m$ . Using this notation, the order of the multivariate autoregressive model is  $p \cdot m$ .

In the multivariate case, the one-step-ahead predictions of the outputs can be obtained starting from the two following matrices: (1) a block row matrix  $\mathbf{A} = [\mathbf{A}_p \ \mathbf{A}_{p-1} \ \dots \ \mathbf{A}_1]$  with dimension  $m \times (m \cdot p)$ , which is a side-by-side collection of  $p$  autoregressive matrices  $\mathbf{A}_i$  (with  $i = p, p-1, \dots, 1$ ), and (2) a block Hankel matrix  $\mathbf{H}_1$  with dimension  $(m \cdot p) \times (l-p)$ , which contains the past values of the outputs

$$\mathbf{H}_1 = \begin{bmatrix} \mathbf{y}(1) & \mathbf{y}(2) & \dots & \mathbf{y}(\ell-p) \\ \mathbf{y}(2) & \mathbf{y}(3) & \dots & \mathbf{y}(\ell-p+1) \\ \vdots & \vdots & \dots & \vdots \\ \mathbf{y}(p) & \mathbf{y}(p+1) & \dots & \mathbf{y}(\ell-1) \end{bmatrix} \quad (8)$$

The one-step-ahead predictions of the outputs can be determined as follows

$$\tilde{\mathbf{H}}_2(\mathbf{A}) = \mathbf{A} \mathbf{H}_1 \quad (9)$$

where  $\tilde{\mathbf{H}}_2(\mathbf{A}) = [\tilde{\mathbf{y}}(p+1, \mathbf{A}) \ \tilde{\mathbf{y}}(p+2, \mathbf{A}) \ \dots \ \tilde{\mathbf{y}}(l, \mathbf{A})]$  is a block row matrix with dimension  $m \times (l-p)$ , which contains the values of the outputs predicted for the different time sequences with a given set of AR parameters in  $\mathbf{A}$ . In the multivariate case, the prediction (or residual) error at time step  $k$  (with  $k = p+1, p+2, \dots, l$ ) is a vector  $\boldsymbol{\varepsilon}(k, \mathbf{A})$  with dimension  $m \times 1$ , where the  $j$ -th component (for  $j = 1 \dots m$ ) is expressed as

$$\varepsilon_j(k, \mathbf{A}) = y_j(k) - \tilde{y}_j(k, \mathbf{A}) \quad (10)$$

Similarly to the univariate case, when dealing with multivariate autoregressive models the least squares method can be employed to estimate the AR coefficients by arranging the measured outputs of the different time series in the block Hankel matrix  $\mathbf{H}_1$  and in the block row matrix  $\tilde{\mathbf{H}}_2$ . Then, the LS estimate  $\hat{\mathbf{A}}$  for the matrix  $\mathbf{A}$  can be obtained as

$$\hat{\mathbf{A}} = \tilde{\mathbf{H}}_2 \mathbf{H}_1^+ \quad (11)$$

As discussed in Brincker and Ventura (2015), the problem of estimating the autoregressive coefficients is overdetermined if  $(l-p) > (m \cdot p)$ . However, due to the unavoidable presence of noise when dealing with real data, in Brincker and Ventura (2015) it is also stated that the procedure works properly if the problem is well overdetermined - i.e.,  $(l-p) \gg (m \cdot p)$ , which is always the case in civil engineering applications. Similar considerations are also applicable for the univariate case where  $m = 1$ .

The cost function in the multivariate case can be expressed using the following equation

$$J(\mathbf{A}) = \frac{1}{l-p} \sum_{j=1}^m \sum_{k=p+1}^l \varepsilon_j(k, \mathbf{A})^2 \quad (12)$$

as shown in Guidorzi *et al.* (2014). Similarly to the univariate AR identification, the selection of the model memory represents an important step. To this purpose, as mentioned in Guidorzi *et al.* (2014), the memory selection criteria formulated for the univariate case can be extended to the multivariate AR identification.

### 3. Proposed MAR-based strategy for damage detection and localization

The goal of the proposed methodology is to identify the presence and location of changes in a given structure that may be related to a damaged state. The method proposed is

based on the analysis of output-only vibration response collected under ambient excitation. Herein, acceleration data is considered, although velocity or displacement measurements can also be employed. In particular, the proposed strategy consists of the following steps:

- Step 1. Formatting the data samples
- Step 2. Identification of the MAR models
- Step 3. Extraction of damage-sensitive feature vectors
- Step 4. Evaluation of damage indices
- Step 5. Damage detection and localization through statistical tests

The top four steps are addressed in a general fashion and are applicable to any structure that can be modeled as a discrete Multi-Degree of Freedom (MDOF) system. Only step 5 of the proposed procedure is structure type-dependent, and, in the present study, it is specifically developed to be applied to shear-type building structures. It is expected that the methodology could be successfully applied to other types of structures, but this will be the object of future research developments.

#### Step 1. FORMATTING THE DATA SAMPLES

The acquisition and the subsequent pre-processing of the data should be planned and executed so to have a training and a testing datasets.

The training dataset, related to the structure in its baseline condition, should consist of  $n$  samples, where “sample” denotes a set of time histories collected at each instrumented location. It is fundamental to have a “rich” training dataset, which collects a diversity of states labeled as undamaged to simulate operational and environmental variability conditions. The higher the number of available samples, the more accurate the identified training statistical model will be.

The testing dataset (i.e., the dataset acquired during the inspection phase, for which the structural condition is unknown), consists of a single sample. However, it is generally convenient to acquire more data, repeating the identification process using different samples of the same structural state, to improve the robustness of the technique.

#### Step 2. IDENTIFICATION OF THE MAR MODELS

Before identifying the MAR model, a proper memory  $p$  should be selected. To this purpose, the mean square error criterion (Simani *et al.* 2003) is employed in this work evaluating the cost functions described in Eq. (12) for increasing memory values. A stabilization of the obtained outcome is expected when the correct model memory is achieved. As stated in Simani *et al.* (2003), the criterion can be useful to find a suitable model memory or, at least, a range of admissible values for the model memory.

According to the proposed strategy, for both the training and testing datasets, the following calculations should be repeated for increasing values of the model memory (i.e., for  $p = 1 \dots p_{max}$ ):

- estimation of the multivariate autoregressive model (i.e., estimation of the block row matrix  $\hat{\mathbf{A}}$ ) using

Eq. (11);

- evaluation of the one-step-ahead predictions and evaluation of the residual errors using Eqs. (9)-(10), respectively;
- determination of the value of the cost function using Eq. (12).

The values of the cost function evaluated for each memory value should be plotted as a function of  $p$  to find the most suitable model memory. During this phase, it is important to check that the cost functions obtained for different samples of the training dataset have similar trends. The maximum memory value considered when repeating the above-mentioned calculations should also be large enough to observe a clear stabilization. According to the proposed strategy for damage detection, the memory of the identified MAR models should be the same for the baseline condition and for the potentially damaged state. The model memory is indeed a parameter that, as shown in the next steps, defines the dimension of the damage-sensitive features vector. This last requirement guarantees that the DSFs related to different states can be properly compared and processed in the proposed method.

Upon selecting the model memory, a block row matrix

$$\hat{\mathbf{A}} = [\hat{\mathbf{A}}_p \ \hat{\mathbf{A}}_{p-1} \ \dots \ \hat{\mathbf{A}}_i \ \dots \ \hat{\mathbf{A}}_1] \quad (13)$$

is derived for each sample by identifying the MAR model. The components of a generic identified AR matrix  $\hat{\mathbf{A}}_i$  are

$$\hat{\mathbf{A}}_i = \begin{bmatrix} \hat{\alpha}_{(1,1),i} & \hat{\alpha}_{(1,2),i} & \dots & \hat{\alpha}_{(1,s),i} & \dots & \hat{\alpha}_{(1,m),i} \\ \hat{\alpha}_{(2,1),i} & \hat{\alpha}_{(2,2),i} & \dots & \hat{\alpha}_{(2,s),i} & \dots & \hat{\alpha}_{(2,m),i} \\ \vdots & \vdots & & \vdots & & \vdots \\ \hat{\alpha}_{(r,1),i} & \hat{\alpha}_{(r,2),i} & \dots & \hat{\alpha}_{(r,s),i} & \dots & \hat{\alpha}_{(r,m),i} \\ \vdots & \vdots & & \vdots & & \vdots \\ \hat{\alpha}_{(m,1),i} & \hat{\alpha}_{(m,2),i} & \dots & \hat{\alpha}_{(m,s),i} & \dots & \hat{\alpha}_{(m,m),i} \end{bmatrix} \quad (14)$$

where the indices  $r, s = 1, 2, \dots, m$  denote the position of each component in the matrix. The parameter  $m$  has been already introduced in Section 2 as the number of time series used for the identification of the MAR model, and, within the proposed MAR-based strategy for damage detection, this parameter coincides with the number of instrumented locations.

#### Step 3. EXTRACTION OF THE DAMAGE-SENSITIVE FEATURE VECTORS

In this step, the vectors collecting the damage-sensitive features are extracted from the identified MAR models. For each component  $\hat{\alpha}_{(r,s),i}$  of the generic identified AR matrix  $\hat{\mathbf{A}}_i$  (Eq. (14)), the elements  $\hat{\alpha}_{(r,s),i}$ , with  $i = p, p - 1, \dots, 1$ , are stored into a vector  $\mathbf{x}_{(r,s)}$ , as follows:

$$\mathbf{x}_{(r,s)} = [\hat{\alpha}_{(r,s),p} \ \hat{\alpha}_{(r,s),p-1} \ \dots \ \hat{\alpha}_{(r,s),i} \ \dots \ \hat{\alpha}_{(r,s),1}]^T \quad (15)$$

This vector, considered here as a damage-sensitive feature, has dimensions  $p \times 1$  and contains the elements of  $\hat{\mathbf{A}}_i$  matrices identified by the index pair  $(r, s)$ . All the components of the AR matrices are considered to form  $m \cdot$

$m$   $\mathbf{x}_{(r,s)}$  with  $r, s = 1, 2, \dots, m$  and can be employed for damage identification. This aspect is one of the main distinctive characteristics of the proposed approach. Indeed, articles available in the existing literature, such as the ones by Mosavi *et al.* (2012) and Loh *et al.* (2016), only use the diagonal components of the identified AR matrices for performing the damage localization task.

In the proposed method, the elements with  $r = s$  (i.e.,  $\mathbf{x}_{(r,r)}$ ) are only representative of the instrumented locations identified with the index  $r (= s)$ . On the other hand, the elements with  $r \neq s$  consist of the off-diagonal terms of the AR matrices and contain mixed information about the  $r$ -th and the  $s$ -th measured DOFs.

The extraction of the DSF vectors has to be performed for all the identified MAR models. At the end of this process, for each index pair  $(r, s)$ ,  $n$  DSF vectors (indicated as  $\mathbf{x}_{B,(r,s),q}$  with  $q = 1 \dots n$ ) are generated for the baseline condition, while – at least – one (indicated as  $\mathbf{x}_{I,(r,s)}$ ) is necessary for the inspection phase.

#### Step 4. EVALUATION OF DAMAGE INDICES

The proposed damage detection strategy is developed by exploiting the outlier analysis tools. A detailed literature review concerning outlier analysis techniques can be found in the textbook by Barnett and Lewis (1994). Among the available procedures, a criterion based on the Mahalanobis distance (Mahalanobis 1936) is adopted herein. This distance metric is used in this work to calculate the damage indices, defined as the distance between the DSF vectors of the baseline and of the inspection phase, as defined in the section above.

The proposed damage index is defined as

$$MD_{(r,s)} = \sqrt{(\mathbf{x}_{I,(r,s)} - \bar{\mathbf{x}}_{B,(r,s)})^T \mathbf{S}_{B,(r,s)}^{-1} (\mathbf{x}_{I,(r,s)} - \bar{\mathbf{x}}_{B,(r,s)})} \quad (16)$$

In Eq. (16) the terms  $\bar{\mathbf{x}}_{B,(r,s)}$  and  $\mathbf{S}_{B,(r,s)}$  are the sample mean vector and the sample covariance matrix of the DSF vectors related to the baseline condition (i.e., the DSF vectors  $\mathbf{x}_{B,(r,s),q}$  with  $q = 1 \dots n$ ), respectively, while the term  $\mathbf{x}_{I,(r,s)}$  is the DSF vector related to the inspection phase. The proposed damage index thus evaluates the Mahalanobis distance in the multivariate space of the considered DSFs between the point related to the inspection phase and the centroid related to the baseline condition. It is worth emphasizing that in Eq. (16) the mean vector and the covariance matrix do not include the DSF vector  $\mathbf{x}_{I,(r,s)}$  (i.e.,  $\bar{\mathbf{x}}_{B,(r,s)}$  and  $\mathbf{S}_{B,(r,s)}$  are exclusive measures). As observed in Farrar and Worden (2013), in SHM applications it is indeed not convenient to “contaminate” the statistics related to the baseline state with the potential outlier related to the inspection phase. Eq. (16) has to be evaluated for each index pair  $(r, s)$ , i.e., for each component of the identified AR matrices. This results in a matrix for each inspection formed by the values of the damage index  $MD_{(r,s)}$  (where  $r, s = 1, 2, \dots, m$ ). Such a matrix is denoted herein as  $MD$  matrix.

It is necessary to underline that, when performing the

calculations using a damage index based on the Mahalanobis distance, the number of samples of the training dataset should be large enough to obtain a reliable statistical model with adequate estimates of the mean vector and of the covariance matrix. This is of paramount importance, especially for the sample covariance matrix, which, as shown in Eq. (16), is subjected to numerical inversion and may become ill-conditioned if the number of samples  $n$  is not large enough (Balsamo and Betti 2015).

#### Step 5. DAMAGE DETECTION AND LOCALIZATION THROUGH STATISTICAL TESTS

As a final step of the proposed vibration-based strategy, statistical tests have to be performed in order to identify the presence and location of modifications in the structure that can be associated with a damaged state. In these statistical tests, the damage indices  $MD_{(r,s)}$  are compared with a threshold value.

For shear-type building structures, it is recommended to perform the statistical tests for all the DOF-related index pairs  $(r, s)$ . For such types of structures, however, some specific index pairs (i.e., the ones with  $r = s$ ,  $r = s - 1$ , and  $r = s + 1$ ) are more informative than others, as shown by the numerical and experimental analyses presented in later sections. The focus should thus be on these index pairs, which means considering the components of the main diagonal (i.e., referred to specific DOFs) and the components of the first diagonal above or below the main one in the  $MD$  matrix (i.e., referred to related interstories of the shear-type building).

According to the proposed strategy, a structural modification – which can be associated with a damaged state and which has affected the dynamics of the structure – is detected if the proposed damage index is

$$MD_{(r,s)} > MD^{TH} \quad (17)$$

for at least one of the DOF-related index pairs  $(r, s)$ , where  $MD^{TH}$  is a threshold value selected as described in Section 3.1. As stated before, multiple samples for each inspection phase should be selected to improve the robustness of the procedure over the occurrence of false alarms. On the other hand, if

$$MD_{(r,s)} \leq MD^{TH} \quad (18)$$

for all the index pairs  $(r, s)$ , then it can be deduced that no structural modifications have occurred in the whole structure. Using the inequalities in Eqs. (17) and (18), it is thus possible to localize structural modifications that can be associated with a damaged state. In general, the obtained  $MD$  matrix should be inspected to identify clusters of components that are above the threshold. The maximum values of the identified clusters can indicate the DOFs that have been mainly affected by eventual structural modifications. Such clusters can be single or multiple clusters, depending on whether single or multiple localized modifications have occurred.

### 3.1 Definition of the threshold for the damage index based on Mahalanobis distance

In this paper, a procedure proposed by Worden *et al.* (2000), Farrar and Worden (2013) to calculate a threshold for discordancy tests in outlier analysis based on the Mahalanobis squared distance is adopted. It is worth noting that a similar approach has also been used in the work by Bernagozzi *et al.* (2018) considering a damage localization strategy and related damage-sensitive features that are different from those considered in this paper.

In the proposed procedure, the threshold value  $MD^{TH}$  is determined through a Monte Carlo simulation, not involving experimental data measured on the structure. Indeed, the threshold only depends on two parameters: the dimension of the DSF vectors used for evaluating the damage indices (i.e., the parameter  $p$ ) and the number of samples of the baseline condition (i.e., the parameter  $n$ ).

The damage detection procedure consists of six main steps, where the last step – not present in the original procedure – has been specifically introduced to deal with the Mahalanobis distance instead of the Mahalanobis squared distance:

T1) A matrix  $\mathbf{Z}$  of dimension  $p \times n$  consisting of random numbers from a univariate normal distribution with a zero mean and a standard deviation equal to 1 is generated. Each column  $\mathbf{z}(i)$ , with  $i = 1 \dots n$ , of the matrix  $\mathbf{Z}$  is a feature vector with dimension  $p \times 1$ . The mean vector  $\bar{\mathbf{z}}$  and the covariance matrix  $\mathbf{S}_z$  of these feature vectors are then calculated.

T2) The Mahalanobis squared distance between each point in the generated multivariate space (i.e., each column  $\mathbf{z}(i)$ ) and the centroid (i.e., the mean vector  $\bar{\mathbf{z}}$ ) is evaluated as

$$MD^2(i) = (\mathbf{z}(i) - \bar{\mathbf{z}})^T \mathbf{S}_z^{-1} (\mathbf{z}(i) - \bar{\mathbf{z}}) \quad (19)$$

The maximum value among the Mahalanobis squared distances  $MD^2(i)$  obtained for  $i = 1 \dots n$  is stored. It is worth noting that each feature vector  $\mathbf{z}(i)$  is included in the calculation of the statistics related to the whole dataset (i.e., the mean vector  $\bar{\mathbf{z}}$  and the covariance matrix  $\mathbf{S}_z$ ). This means that inclusive measures of the Mahalanobis squared distance are obtained using Eq. (19).

T3) The steps T1 and T2 are repeated several times, by considering a number of trials that is at least equal to 1000, as recommended in Farrar and Worden (2013). For each trial, as anticipated at step T2, the maximum value of Mahalanobis squared distance is stored, forming a vector  $\mathbf{v}$  containing all the maximum values of the Mahalanobis squared distance.

T4) The  $w$ -th percentile of the values contained in the vector  $\mathbf{v}$  is then determined. The parameter  $w$  is typically selected equal to 95 or 99 (Farrar and Worden 2013): in this paper,  $w = 99$  was selected. The value of the threshold obtained at this step represents an inclusive threshold, denoted by the symbol  $T_{inc}$ .

T5) The exclusive threshold (denoted as  $T_{exc}$ ) is obtained from the inclusive threshold estimated at step T4, as follows

$$T_{exc} = \frac{(n-1)(n+1)^2 T_{inc}}{n(n^2 - (n+1)T_{inc})} \quad (20)$$

It is worth noticing that this step is required since in the proposed MAR-based strategy, as shown in Eq. (16), the statistics related to the baseline state are evaluated as exclusive measures.

T6) The threshold value for the proposed damage index based on Mahalanobis distance is then evaluated as follows

$$MD^{TH} = \sqrt{T_{exc}} \quad (21)$$

The adoption of the Mahalanobis distance in place of the corresponding squared value has shown to offer a damage index that tends to be more proportional to the damage severity.

### 3.2 An alternative damage metric used in the analyses

In this study, as an alternative to the Mahalanobis distance, the Euclidean distances between the DSF vectors were considered as damage indicators. Such values were computed as

$$\begin{aligned} ED_{(r,s)} &= \|\mathbf{x}_{I,(r,s)} - \bar{\mathbf{x}}_{B,(r,s)}\|_2 \\ &= \sqrt{(\mathbf{x}_{I,(r,s)} - \bar{\mathbf{x}}_{B,(r,s)})^T (\mathbf{x}_{I,(r,s)} - \bar{\mathbf{x}}_{B,(r,s)})} \end{aligned} \quad (22)$$

In Eq. (22), the operator  $\|\cdot\|_2$  denotes the 2-norm operator and, similarly to the damage metric based on Mahalanobis distance (Eq. (16)), the index based on Euclidean distance can be evaluated for each index pair  $(r, s)$ . A matrix (denoted as  $ED$  matrix) formed by  $ED_{(r,s)}$  values (where  $r, s = 1, 2, \dots, m$ ) can thus be obtained for each inspection phase. From the comparison between Eqs. (16)-(22), the two aforementioned metrics differ because the sample covariance matrix is not present in the formulation of the Euclidean distance. Hence, the Euclidean distance option may be more suitable than the Mahalanobis-based metric for applications with small training datasets. However, these more challenging scenarios are not part of the objectives of the present paper, and Euclidean-based damage indices are herein evaluated solely to obtain more insight into the damage identification process.

## 4. Results

In this section, two case studies are presented to test the performance of the proposed damage identification strategy. In the first case study, the simulated acceleration response of a 5-DOF shear-type system is used to determine the occurrence and location of damage for different scenarios. The second case study exploits the acceleration response of

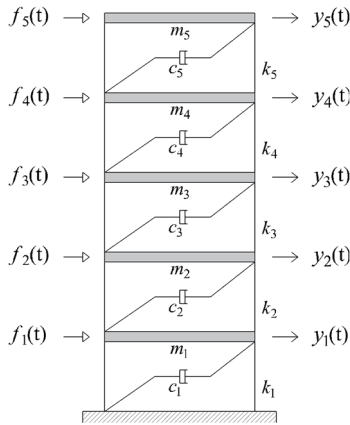


Fig. 1 Test structure for case study 1

a scaled building model available at the Engineering Institute of the Los Alamos National Laboratory (Figueiredo *et al.* 2009).

#### 4.1 Case 1: Simulated shear-type system

**System description.** The numerically simulated system is a 5-story shear-type system (Fig. 1), built according to the common lumped mass–spring–viscous damper chain, where the energy dissipation properties are modeled according to the Rayleigh damping mechanism and the corresponding damping coefficients are indicated with  $c_j$ . The masses  $m_j$  ( $j = 1, 2, \dots, 5$ ) are numbered in ascending order so that the mass closest to the constraint is labeled as 1. The interstory stiffness between the  $(j - 1)$ -th and the  $j$ -th masses is denoted as  $k_j$ . The baseline system is characterized by interstory stiffness,  $k_j^0 = 25000 \text{ N/m}$  and mass  $m_j^0 = 1 \text{ kg}$  with  $j = 1, \dots, 5$ .

The system is subjected to a white Gaussian input of mean zero and standard deviation one applied at each DOF, indicated as  $f_j(t)$  in Fig. 1. The simulated acceleration response time histories of the system are 5 minutes long, sampled at 0.005 s. Three sets of simulations are carried on considering different Root Mean Square (RMS) levels of corrupting noise (1%, 5% and 10%), that are added to the system response in order to mimic the effects of measurement noise and to evaluate its influence on the proposed procedure. For the present case study, the acceleration response time histories are collected in fourteen different structural conditions: one undamaged and thirteen addressed as “damaged”, where modifications either to the masses or the stiffnesses of the system are introduced (Table 1).

**Feature extraction and training.** At the core of the damage detection strategy, the training set is built over 200 sets of time histories (i.e., the aforementioned “samples”) simulated for the baseline condition. Therefore, the training dataset is constituted by  $200 \times m$  time histories, where  $m$  is the number of simulated accelerometers. In the following case study, a full set of sensors is considered, where the acceleration response of the system is available at each mass. Other more challenging scenarios characterized by

Table 1 Damaged and undamaged states considered for case study 1

State	Condition	Description
1	Undamaged	Baseline
2	Damaged	$m_1 = 1.2 m_j^0$
3	Damaged	$m_3 = 1.2 m_j^0$
4	Damaged	$m_4 = 1.2 m_j^0$
5	Damaged	$k_1 = 0.85 k_j^0$
6	Damaged	$k_2 = 0.85 k_j^0$
7	Damaged	$k_3 = 0.85 k_j^0$
8	Damaged	$k_5 = 0.85 k_j^0$
9	Damaged	$k_3 = 0.90 k_j^0$
10	Damaged	$k_3 = 0.80 k_j^0$
11	Damaged	$k_3 = 0.90 k_j^0$ and $k_4 = 0.90 k_j^0$
12	Damaged	$k_2 = 0.90 k_j^0$ and $k_3 = 0.90 k_j^0$
13	Damaged	$k_2 = 0.90 k_j^0$ and $k_5 = 0.90 k_j^0$
14	Damaged	$k_2 = 0.90 k_j^0$ and $k_3 = 0.80 k_j^0$

incomplete sensor setups do not represent the key interest in the present study and will be addressed in future works.

The model memory used in the identification of the MAR model is established by investigating the trend of the cost function, as explained in the Step 2 of the procedure proposed in this work. Fig. 2 shows the cost functions derived for memory values up to 30. In particular, in Fig. 2(a), 10 trends are shown, representing the cost functions evaluated considering 10 samples of the baseline condition. On the other hand, in Fig. 2(b), 14 trends referring to single samples of the inspection conditions are reported (one for each tested scenario in Table 1). The overall behavior of the cost function remains consistent for all the samples, both in the training analysis and in different structural conditions. The function presents a substantial drop at memory values equal to 2-3, and then it slowly stabilizes. Therefore, in the analyses, the memory has been selected equal to 3, which leads to a block row matrix  $\hat{\mathbf{A}}$  (Eq. (13)) of dimensions  $5 \times 15$ .

Starting from the extracted block row matrix, the MAR coefficients are then collected in 25 vectors  $\mathbf{x}_{(r,s)}$ , one for each component  $\hat{\alpha}_{(r,s),i}$  (Eq. (15)), from which the sample mean vector and the sample covariance matrix are derived.

The threshold value for the Mahalanobis distance adopted in the damage detection strategy for the numerical simulation is derived according to the Monte Carlo procedure outlined in Section 3.1. Considering a memory equal to 3, 200 sets of time histories in the training phase, 1000 running trials and a 99 percentile, the threshold value of the Mahalanobis distance is estimated to be 3.85.

**Testing.** To test whether the algorithm is capable of identifying the presence of structural damage, 50 time histories of the system response at each DOF and all the fourteen states (Table 1) are simulated. For the single sample, 25 feature vectors  $\mathbf{x}_{I,(r,s)}$  are extracted and used to compute the corresponding damage indices  $MD_{(r,s)}$ .

The results for the 50 time histories and for different

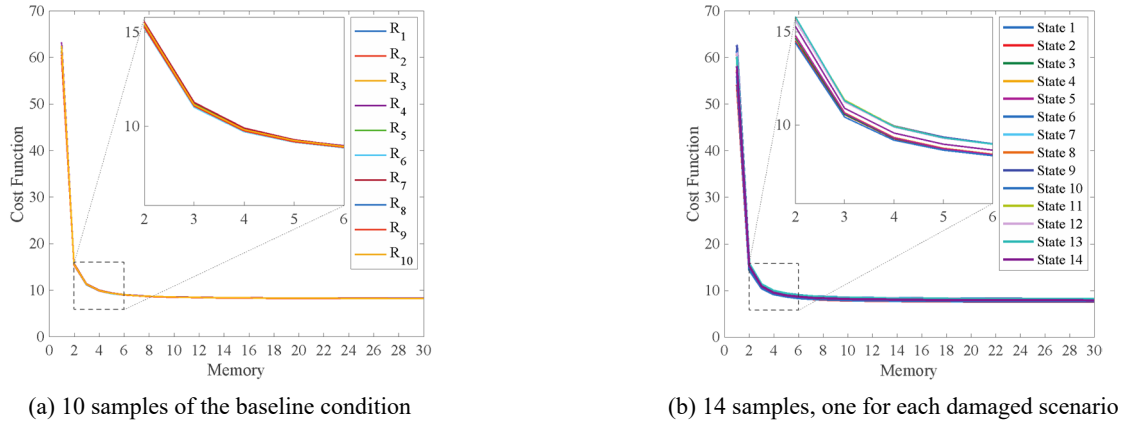


Fig. 2 Cost function for MAR model for case study 1

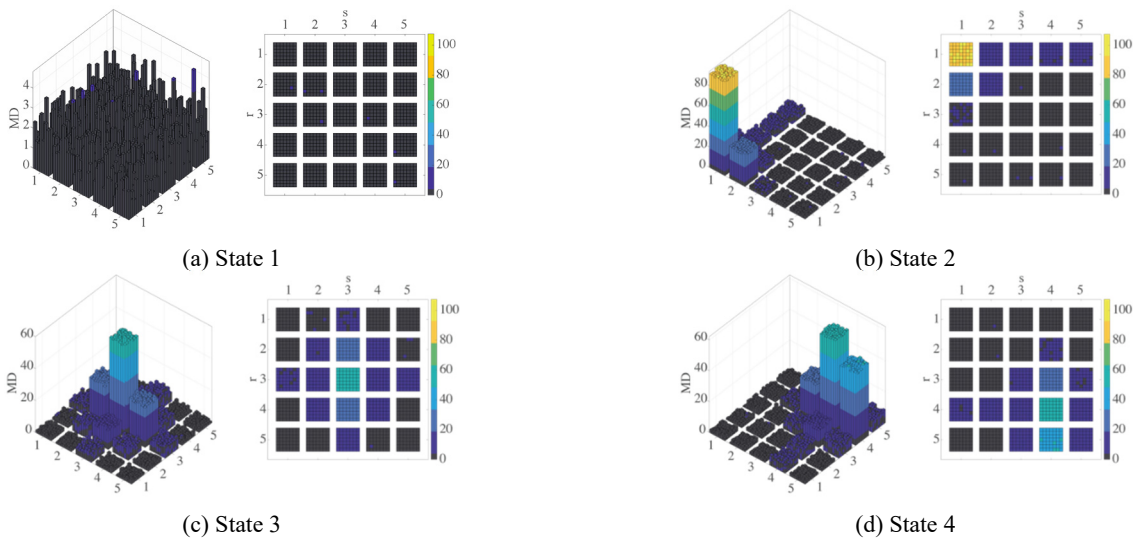


Fig. 3 MD matrix for tests of case study 1

damage scenarios are here discussed adopting a color bar representation of the  $MD$  matrices. Each figure is associated with a tested state (Table 1) and shows a set of  $m \times m$  matrices ( $5 \times 5$  for the numerical case study) where the generic  $(r, s)$  element collects the Mahalanobis distances,  $MD_{(r,s)}$ , computed in the tested samples simulated for that damage scenario.

The bar colors address the classification in damaged or undamaged state. The samples classified as undamaged present Mahalanobis values that lay under the threshold and are characterized by dark grey color. Samples classified as damaged are instead associated with a color scale varying from blue to yellow with increasing values of the Mahalanobis distance.

Fig. 3(a) shows the results for the undamaged tested scenario considering the 10% level of noise. All the simulated samples lead to Mahalanobis distance values that fall below the threshold that discriminates between healthy and unhealthy conditions, except for three samples. Almost all the inspected records are correctly associated with the undamaged system, highlighting the robustness of the procedure in high noise level conditions.

Figs. 3(b)-(d) show the results for the damaged states

(#2-4) considering a 10% noise corruption of the acceleration response time histories. In these scenarios, an additional mass corresponding to the 20% of the one adopted in the baseline is added to a different degree of freedom. All these conditions cause a substantial modification of the MAR coefficients located along the main diagonal of the identified AR matrices  $\hat{A}_i$  at the position  $(j, j)$ , where the additional mass is added. This variation is reflected in the damage index  $MD_{(j,j)}$  which exceeds the threshold and presents the maximum value among all the elements on the diagonal. The coefficients lying on the  $j$ -th row are also influenced by the mass perturbation and overpass the threshold and the same applies to some of the coefficients located on the  $j$ -th column, particularly for the ones placed right above and below the interested one. This behavior can be explained by understanding the role played by the MAR coefficients. The  $j$ -th row of the  $MD$  matrix collects all the indices related to the coefficients that take into account the influence of the remaining DOFs on the  $j$ -th DOF response regression. On the other hand, the  $j$ -th column collects all the damage indices associated with the coefficients that consider the influence of the  $j$ -th DOF on the remaining DOFs.

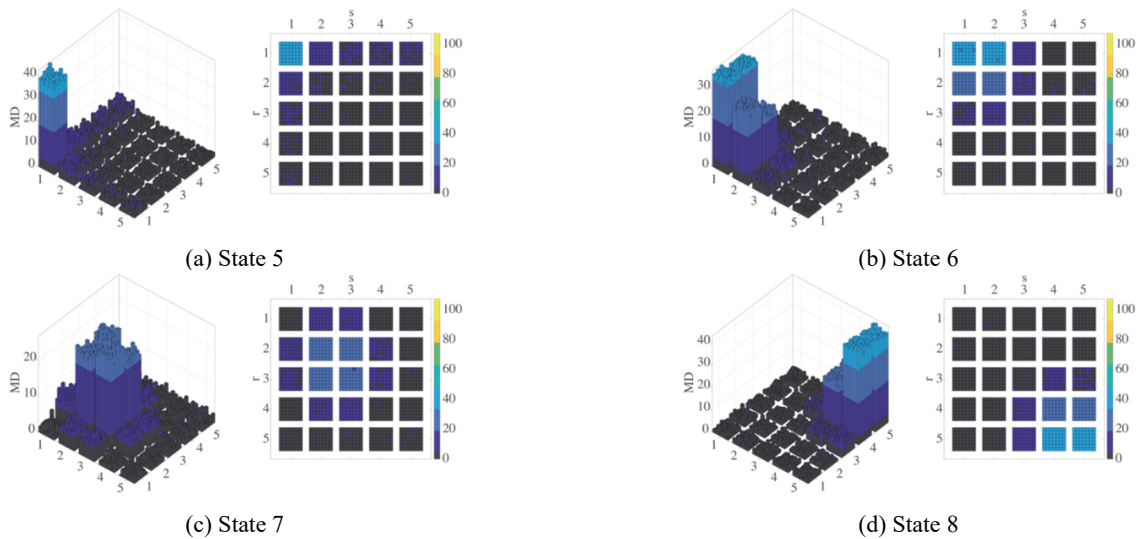


Fig. 4 MD matrix for tests of case study 1

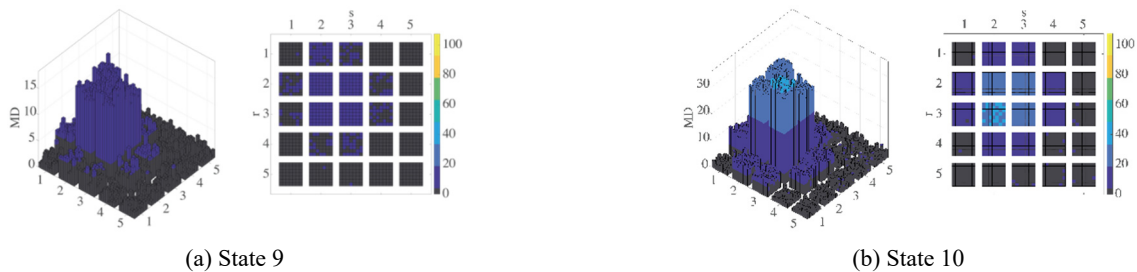


Fig. 5 MD matrix for tests of case study 1

Therefore, if the damage occurs at the  $j$ -th DOF, the coefficients that consider the influence from and on the  $j$ -th DOF itself are those that more likely show that variation. The other coefficients remain substantially unchanged presenting Mahalanobis distances below the threshold, confining the DOF interested by damage and giving information that help the damage localization.

It is evident that not all the coefficients are influenced in the same way. Excluding the damage index  $MD_{(j,j)}$ , which shows the maximum variation, the neighboring damage indices present dissimilar values, like  $MD_{(2,1)}$  and  $MD_{(1,2)}$  in state 2 or  $MD_{(3,4)}$  and  $MD_{(5,4)}$  in state 4. This behavior is accentuated when the additional mass is placed at stories close either to the base or to the top level of the shear-type system, where the boundary conditions influence the system response. The Mahalanobis distance metric happens therefore to account the influence of the boundary conditions on the system response.

A different pattern in the damage indices can be observed, as shown in Fig. 4, when a stiffness reduction at the  $j$ -th interstory,  $k_j$ , between the  $(j - 1)$ -th and the  $j$ -th DOFs is introduced. The main variations are observed for the damage indices  $MD_{(j,j)}$  and  $MD_{(j-1,j-1)}$  located along the principal diagonal of the damage matrix  $MD$ . This is expected because any variation at the interstory stiffness affects the MAR coefficients directly playing a role in the regression of the acceleration responses of the two

DOFs located closer to the interested interstory. In addition to the elements on the principal diagonal, also the elements off-diagonal at position  $(j, j - 1)$  and  $(j - 1, j)$  show similar variations, being associated with the MAR coefficients that take into account the influence of the  $j$ -th DOF on the  $(j - 1)$ -th DOF and vice versa. The asymmetries observed for the damage cases associated with an additional mass can also be found for the stiffness reductions.

It is interesting to see how the intensity of damage is reflected in the magnitude of the damage index. Fig. 5 shows the Mahalanobis distance matrices for the damage states 9 and 10, where the interstory stiffness,  $k_3$ , is reduced by 10% and 20%, respectively. Considering also the results for state 7, where the same stiffness was reduced by 15%, it can be noticed that, increasing the damage level, the maximum observed value of the damage index also increases (18.25, 26.64 and 35.84).

The robustness of the proposed damage detection and localization strategy has also been tested considering double-damage scenarios. Fig. 6 shows the results for those cases in which damage occurs at two different locations (damage states 11, 12, 13, and 14).

When the stiffness reduction is introduced into two consecutive interstories (states 11, 12 and 14)  $k_j$  and  $k_{j+1}$ , the damage index showing the maximum value is  $MD_{(j,j)}$  which corresponds to the coefficient associated with the

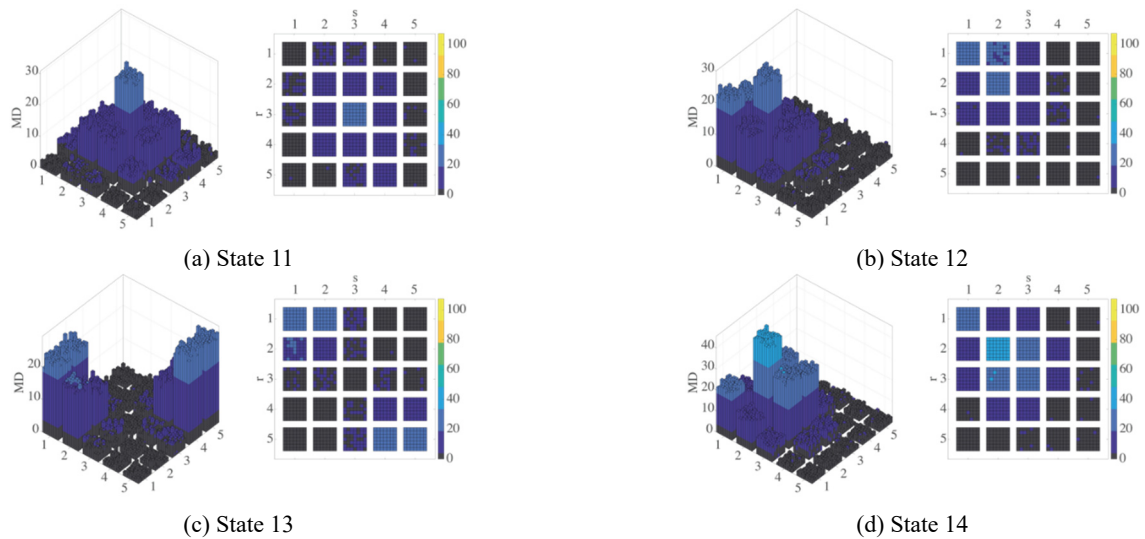


Fig. 6 MD matrix for tests of case study 1

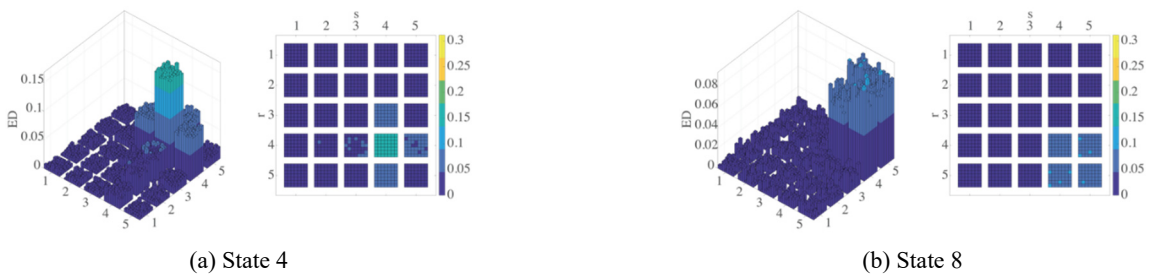


Fig. 7 ED matrix for tests of case study 1

DOF common to both the interstories. In addition, the damage also affects the elements  $MD_{(j-1,j-1)}$  and  $MD_{(j+1,j+1)}$  on the main diagonal and the off-diagonal elements  $MD_{(j,j-1)}$ ,  $MD_{(j-1,j)}$ ,  $MD_{(j,j+1)}$ ,  $MD_{(j+1,j)}$ ,  $MD_{(j-1,j+1)}$ , and  $MD_{(j+1,j-1)}$ , which show smaller values with respect to  $MD_{(j,j)}$ , but all above the threshold. The proposed damage assessment strategy also performs well when considering double-damage scenarios where the stiffness reduction is imposed on two non-consecutive interstories. In state 13, the second and fifth interstories face a 10% reduction of stiffness. In this damage scenario, only the damage indices associated with the coefficients related to those interstories are affected, demonstrating the effectiveness of the strategy in the damage localization. The observed trend manifests accordingly, also considering damaged scenarios in which the reduction of stiffness in the two consecutive interstories is not uniform (Fig. 6(d)). In these conditions, the damage index magnitude reflects the damage intensity, showing the same damage pattern observed for the double-damage conditions.

As mentioned in Section 3.2, it is possible to consider alternative metrics to define the damage index. A common alternative to the Mahalanobis distance is the Euclidean distance. Fig. 7 shows the results considering this second distance metric for states 4 and 8. It is evident how the overall behavior of the damage indices remains unvaried, confirming the applicability of the proposed damage assessment strategy even with different metrics.

It is worth noticing that the damage indices given in terms of Euclidean distance are more uniform in comparison with those obtained considering the Mahalanobis distance. This distinction in the behavior can be attributed to the different nature of the two metrics. Indeed, the Euclidean distance assumes the data to be generated from an isotropic Gaussian model. On the other hand, the Mahalanobis distance seeks to measure the correlation between variables and relaxes the Euclidean distance assumption, assuming an anisotropic Gaussian distribution instead. Therefore, the adoption of the Mahalanobis distance as metric in the damage detection strategy provides additional information on how the DSFs relate to each other and how the damage influences them differently.

The effects of measurement noise on the damage classification have been tested considering three RMS levels of corrupting noise: 1%, 5%, and 10%. As an example, Fig. 8 presents the box plot (showing medians, quartiles and maximum-minimum values) for the damage indices  $MD_{(3,3)}$  and  $MD_{(5,1)}$  considered at two different damage scenarios, state 1 and state 7, computed with three measurement noise levels. The two indices present a consistent distribution between the three noise levels over the 50 simulated realizations in the undamaged scenario. When the stiffness at the third interstory is reduced, the damage index  $MD_{(5,1)}$ , away from the critical position in the MD matrix, remains almost identical and does not

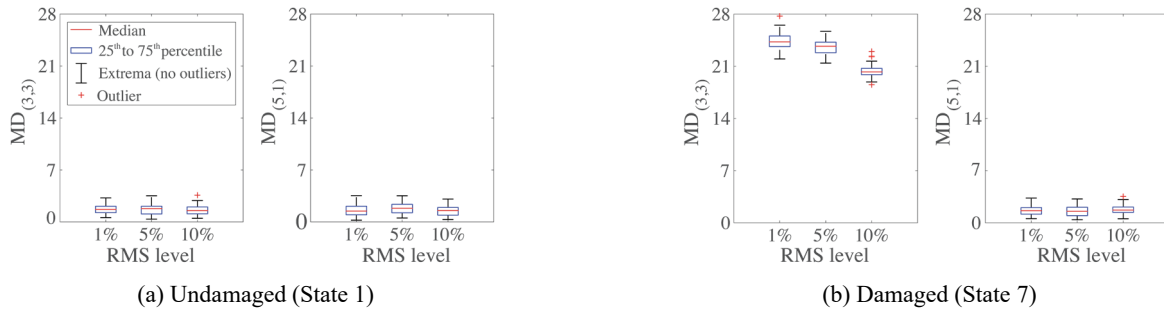


Fig. 8 Box plot for case study 1 considering different RMS noise levels (1%, 5%, and 10%)



Fig. 9 MD values for State 7 for case study 1

show substantial differences for the different noise levels. On the contrary, referring to the index  $MD_{(3,3)}$ , which is associated with the MAR coefficient related to the DOF affected by damage, the introduction of different noise levels induces a perturbation in the damage index magnitude. This perturbation is, however, small in comparison with the damage index value, and consequently it does not endanger the detection and localization task.

The proposed damage detection and localization strategy is robust in several scenarios and could offer improvements, particularly towards the localization task, compared with methodologies built on the univariate autoregressive models.

The univariate regression model is built considering the system time histories recorded at each sensor individually, estimating  $m$  individual row matrices  $\hat{a}$  (Eq. (6)) of dimension  $1 \times p$ . Therefore, in this case, an  $MD$  vector of dimensions  $m \times 1$  is computed in place of the  $MD$  matrix derived in the case of the MAR model. To appreciate the comparison between the presented strategy built over the MAR model and the corresponding one associated with the UAR model, only the damage indices located on the main diagonal of the damage matrix  $MD$  derived from the MAR model should be considered. These are the damage indexes that show the influence of the  $j$ -th DOF on the structural response of the same DOF, and that can be put in direct comparison with the elements of the  $MD$  vector derivable in the case of the UAR model.

In this case study, the AR coefficients in the univariate model are computed adopting a model memory equal to 17.

The memory is inferred implementing the same approach suggested for the multivariate methodology, and the cost function is estimated considering the response time history of each DOF independently from the others. The threshold re-calibrated considering a memory of 17, results equal to 6.57.

Fig. 9 presents the results obtained in the proposed strategy considering the multivariate model, as well as a univariate model, respectively, for state 7. In the case of the UAR model (Fig. 9(a)), the 5 subplots represent the corresponding 5 damage indicators collected in the  $MD$  vector for the 50 realizations simulated for that damage state. In the case of the MAR model (Fig. 9(b)), the 5 subplots show the Mahalanobis distances associated with  $(r, s)$  elements of the  $MD$  matrix where  $r = s$ , in the tested samples simulated for that damage scenario. In both cases, the bar colors address the same classification in damaged or undamaged state presented for the 3D representation previously given.

In the univariate approach, the damage detection task is correctly achieved but the localization of the damaged area cannot be accomplished since all the indices exceed the threshold and assume similar magnitudes. On the contrary, in the multivariate methodology, only the damage indices  $MD_{(2,2)}$  and  $MD_{(3,3)}$  overshoot the threshold, while the others consistently fall below, indicating that the occurrence of damage is between the 2<sup>nd</sup> and 3<sup>rd</sup> DOF and thus demonstrating the superiority of the proposed method over the univariate approach. Further comparisons between the proposed MAR-based method and other existing methods,

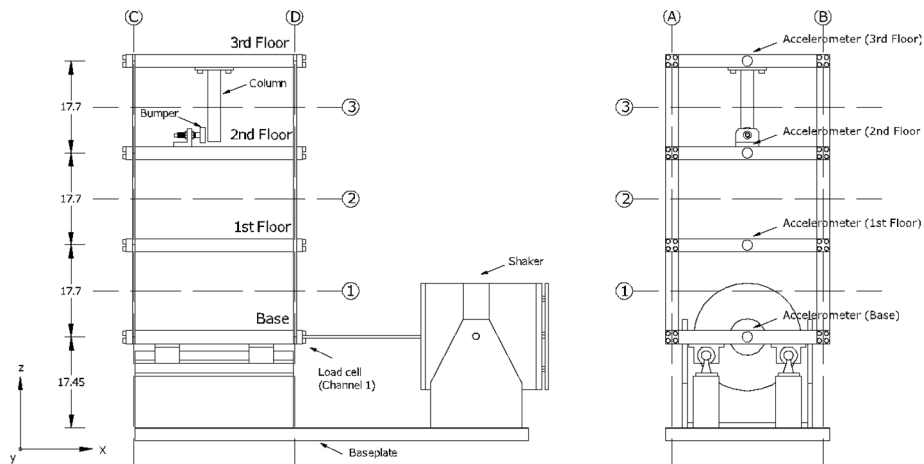


Fig. 10 Test structure for case study 2 (adapted from Figueiredo *et al.* 2009); dimensions in cm

Table 2 Damaged and undamaged states considered for case study 2

State	Condition	Description
1	Undamaged	Baseline
2	Damaged	Added mass of 1.2 kg at the 1 <sup>st</sup> floor
3	Damaged	87.5% stiffness reduction in one column of the 1 <sup>st</sup> interstory
4	Damaged	87.5% stiffness reduction in two columns of the 1 <sup>st</sup> interstory
5	Damaged	87.5% stiffness reduction in one column of the 2 <sup>nd</sup> interstory
6	Damaged	87.5% stiffness reduction in two columns of the 2 <sup>nd</sup> interstory
7	Damaged	87.5% stiffness reduction in one column of the 3 <sup>rd</sup> interstory
8	Damaged	87.5% stiffness reduction in two columns of the 3 <sup>rd</sup> interstory

for example based on a different type of DSFs, will be addressed in dedicated future works.

#### 4.2 Case 2: Experimental laboratory model

*System description.* The second case study is a laboratory three-story frame with a moving base, whose schematics and sensor locations are shown in Fig. 10. The reader is referred to Figueiredo *et al.* (2009) for a more detailed description of the structure and of the collected data.

The load is applied by means of an electrodynamic shaker to the base floor along the centerline of the frame. The system is instrumented with four accelerometers mounted at the centerline of each floor and of the base on the opposite side of the excitation source. The dynamic response is sampled at 320 Hz for a duration of 25.6 seconds. The input time history is a band-limited excitation in the range of 20–150 Hz applied at the base and the acceleration response time histories, including the one at the base, are recorded for different structural configurations.

In this study, eight different sample sets were considered, as reported in Table 2. One dataset is obtained from the model in its original configuration, representing the baseline condition for the “healthy” reference condition, while the other seven datasets corresponds to modifications of the mass and stiffness of the structural elements.

*Feature extraction and training.* The training dataset is built over 10 sets of time histories performed to establish the baseline condition. For case study 2, as it was for the previous numerical example, the construction of the training model requires only the evaluation of the sample mean vector and the sample covariance matrix of the features extracted from the training data.

As before, the memory of the system is determined by investigating the cost function trend. Fig. 11 shows the cost functions derived for the 10 samples of the training set (Fig. 11(a)) and one for each tested scenario (Fig. 11(b)). The overall cost function shows a substantial drop at the memory order equal to 2 and then slowly converges to a stable value. Hence, a value of the model memory equal to 2 has been selected for all the analyses, leading to a block row matrix  $\hat{A}$  of dimensions  $4 \times 8$ . Consequently, 16 feature vectors are extracted for every sample in the training set following the same procedure described for the simulated system.

The acceleration response of the base is considered in the construction of the regression model and, consequently, in the extraction of the MAR coefficients both in the training model and in the tested samples. However, being the input excitation directly applied to the base of the structure, the results related to the base level are not reported in the analyses. Considering a memory equal to 2, 10 sets of time histories for training the model, 1000 running trials, and a 99 percentile, the threshold value for the Mahalanobis distance metric has been determined equal to 3.06.

*Testing.* The test dataset consists of 9 samples for each tested scenario (Table 2) for a total of 72 time histories at each recording location. Again, each sample will be considered separately to test the algorithm ability to distinguish between an undamaged or damaged state. Fig.

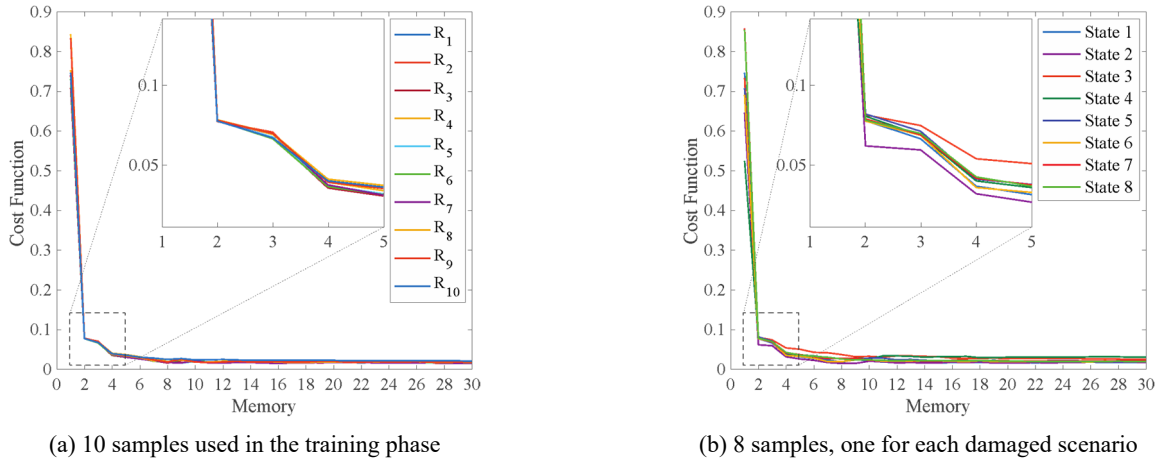


Fig. 11 Cost function for MAR model for case study 2

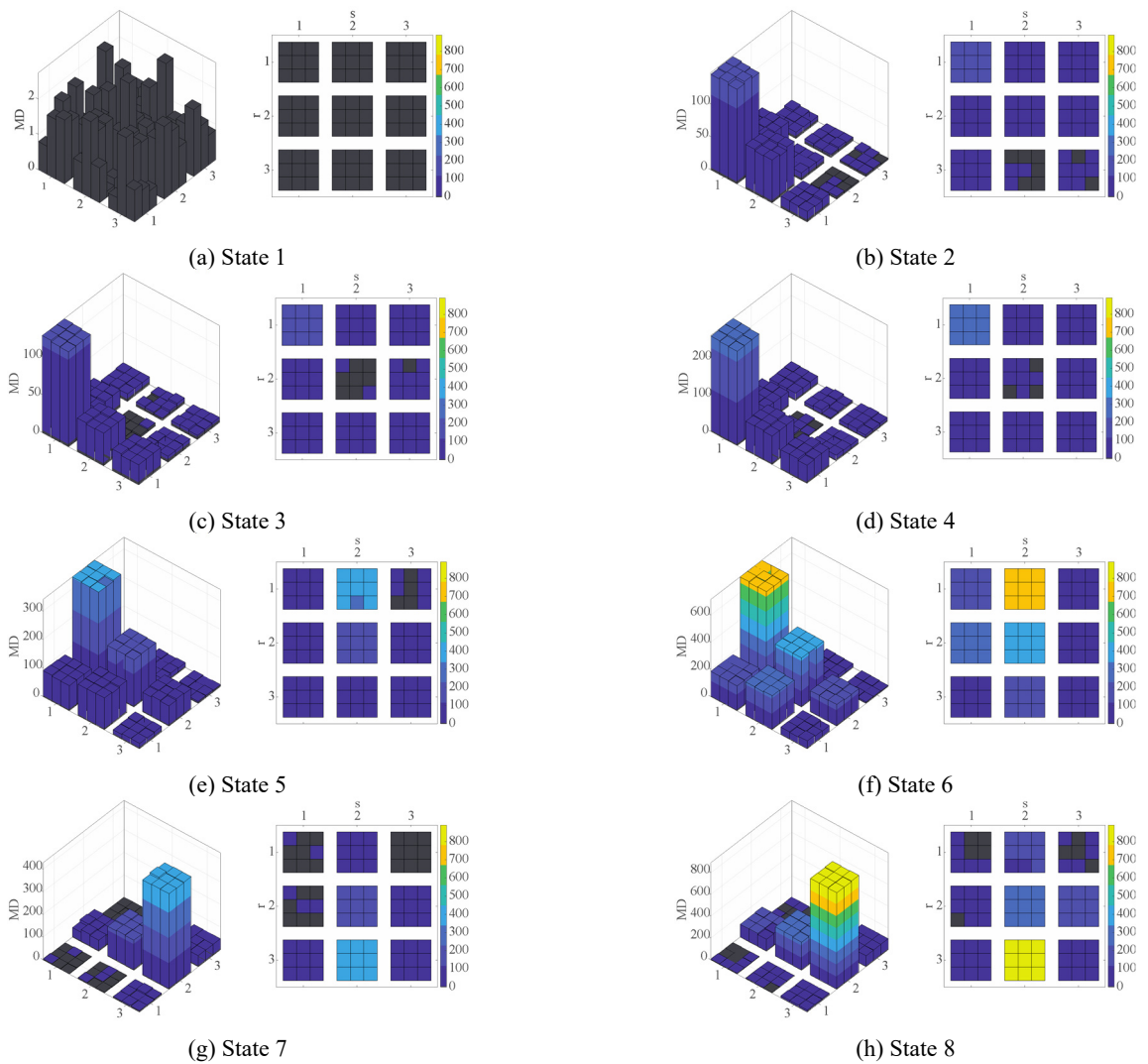


Fig. 12 MD matrix for tests of case study 2

12 shows the results of the proposed strategy and each sub-figure shows a 3×3 set of matrices collecting the Mahalanobis distances  $MD_{(r,s)}$  computed for the  $(r,s)$  coefficient in the 9 tested samples recorded for that damage scenario. All the samples belonging to the undamaged

condition are below the threshold value (Fig. 12(a)), and they are correctly associated with the healthy system. The scenario that involves the additional mass at the first floor, state 2 (Fig. 12(b)), presents, as expected, the highest values of Mahalanobis distance, for all the samples, at position

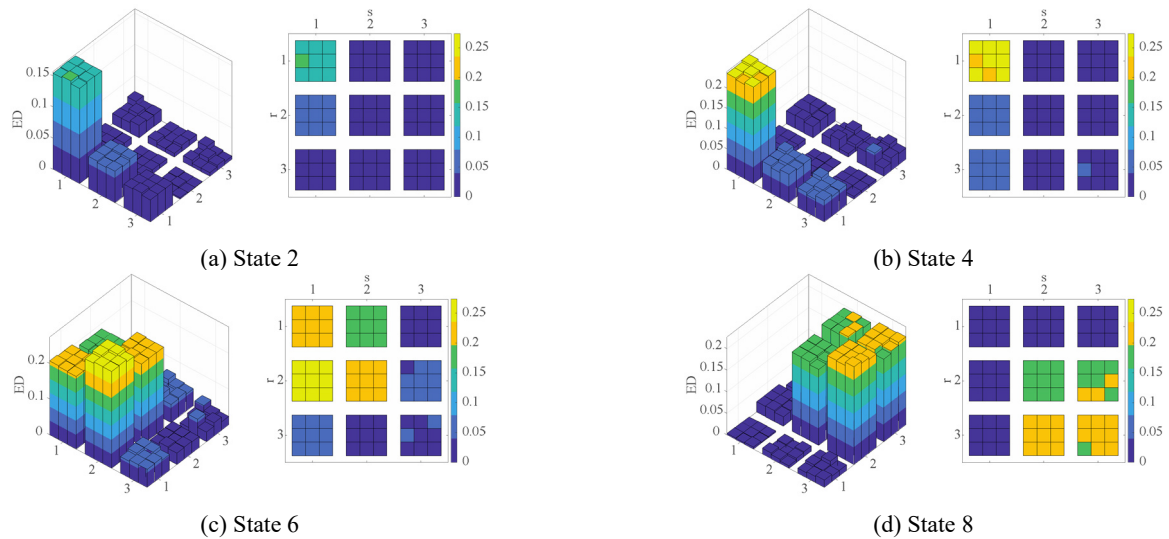


Fig. 13  $ED$  matrix for tests of case study 2

(1,1) in the damage matrix  $MD$ . As in the previous case study, the elements along the first row and the first column tend to be higher than the other indices but smaller than  $MD_{(1,1)}$ . In this condition, some false alarms are registered with indices slightly higher than the threshold but still distinctly smaller than the ones associated with the affected DOFs, thus not penalizing the localization task. This instability in the identification may be partially caused by the small dataset available for the training.

With regards to the cases of damage associated with a stiffness reduction, for states 3 and 4, where the reduction is at the first interstory, the stiffness reduction at the first interstory is clearly visible in the index at position (1,1), where the maximum value of the damage index emerges (Figs. 12(c)-(d)). Considering two different damage intensities, the position of maximum affected coefficients stays the same, and the intensity of the index results to be directly proportional to the introduced damage level.

The states associated with a reduction of stiffness at the second interstory (states 5 and 6) and third interstory (states 7 and 8) emerge with the same previously observed pattern, involving four adjacent elements of the  $MD$  matrix. Again, the stiffness reduction at the  $j$ -th interstory,  $k_j$ , between the  $(j-1)$ -th and the  $j$ -th DOFs causes large variations in the damage indices  $MD_{(j,j)}$ , and  $MD_{(j-1,j-1)}$  as well as on the off-diagonal elements at position  $(j, j-1)$  and  $(j-1, j)$ .

Even if the overall observed behavior agrees with the one seen in the numerical simulation, unlike in the 5-DOF system, there is a strong asymmetry between the four involved elements in the damage scenarios associated with a reduction of stiffness. In this experimental case, the maximum damage index is observed in one of the off-diagonal elements, while in the numerical study, even if asymmetric in some of the damage scenarios, the maximum damage index is consistently observed on the principal diagonal as well.

When considering the Euclidean distance as damage metric, the results present the same overall behavior,

perhaps with a more uniform trend between the indices. Fig. 13 shows the results considering this alternative distance. It is evident how the detection and localization of damage can be inferred from the bar plots. In states 2 and 4 the maximum damage index occurs at position (1,1), indicating that structural modifications (additional mass and reduction in stiffness) occur in the proximity of the first level, confirming the trend observed when considering the Mahalanobis distance.

In states 6 and 8, where damage occurs at the 2<sup>nd</sup> and 3<sup>rd</sup> interstory columns, respectively, the maximum damage index is still on an off-diagonal element but the three neighboring indices associated with the interested DOFs show a value similar to the maximum one. The imbalance observed in the values obtained using the Mahalanobis distance can be attributed to the fact that the Mahalanobis distance allows to better appreciate the correlation between the AR coefficients and the different influence that the damage has on those, while the Euclidean distance, lacking the covariance matrix in its formulation, cannot address this level of detail.

## 5. Conclusions

The present study addresses a novel damage detection and localization strategy based on the use of autoregressive coefficients, derived for a multivariate formulation, as damage-sensitive features. An extensive description of the extraction modality of such features is presented, explaining the approach followed to define the system memory, the extraction process of the AR coefficients, and the damage detection strategy. The proposed methodology adopts the Mahalanobis distance as damage index to investigate the deviation of the AR coefficients corresponding to an unknown condition from those related to the healthy reference model of the system. The definition of the threshold to discriminate between undamaged and damage conditions is determined through numerical calculations based on a Monte Carlo simulation.

The proposed methodology was tested on data from two frame structures. The first test adopted a set of simulated data from a 5-DOF shear-type system, while, in the second test, the experimental data obtained from a scaled building model were used. In the numerical case, the results showed that the proposed damage diagnosis, even in the presence of high levels of measurement noise, is capable of recognizing damaged scenarios from the healthy conditions. In addition, the proposed methodology was quite successful in locating the damaged area, considering a wide range of different simulated conditions: variations in terms of mass and reduction of stiffness in single or double positions. In all the analyses, the damage indices showing the larger deviations from the baseline conditions are those associated with the MAR coefficients strictly related to the damaged DOF, confining the damage location on the system. Similar results were obtained when the proposed methodology was tested on an experimental case study, showing the robustness of the strategy even in handling smaller training datasets. The flexibility of the methodology to different damage index metrics was tested by replacing the Mahalanobis distance with the Euclidean distance: identical conclusions were reached. The performed numerical simulations and experimental validation suggest that the proposed procedure is robust and might be well suited for real-life applications.

## Acknowledgments

The authors would like to acknowledge the Engineering Institute at Los Alamos National Laboratory for making available to the public domain the experimental data used in this work, and downloadable from <http://institute.lanl.gov/ei/software-and-data/>.

## References

- Akaike, H. (1974), "A new look at the statistical model identification", *IEEE Transact. Automatic Control*, **19**(6), 716-723. <https://doi.org/10.1109/TAC.1974.1100705>
- Balsamo, L. and Betti, R. (2015), "Data-based structural health monitoring using small training datasets", *Struct. Control Health Monitor.*, **22**(10), 1240-1264. <https://doi.org/10.1002/stc.1744>
- Barnett, V. and Lewis, T. (1994), *Outliers in Statistical Data*, (3rd Edition), John Wiley & Sons, Chichester, UK.
- Bernagozzi, G., Mukhopadhyay, S., Betti, R., Landi, L. and Diotallevi, P.P. (2018), "Output-only damage detection in buildings using proportional modal flexibility-based deflections in unknown mass scenarios", *Eng. Struct.*, **167**, 549-566. <https://doi.org/10.1016/j.engstruct.2018.04.036>
- Bodeux, J.B. and Golinval, J.C. (2003), "Modal identification and damage detection using the data-driven stochastic subspace and VARMA methods", *Mech. Syst. Signal Process.*, **17**(1), 83-89. <https://doi.org/10.1006/mssp.2002.1543>
- Brincker, R. and Ventura, C.E. (2015), *Introduction to Operational Modal Analysis*, John Wiley & Sons, Chichester, UK.
- Das, S., Saha, P. and Patro, S.K. (2016), "Vibration-based damage detection techniques used for health monitoring of structures: a review", *J. Civil Struct. Health Monitor.*, **6**, 477-507. <https://doi.org/10.1007/s13349-016-0168-5>
- De Stefano, A., Sabia, D. and Sabia, L. (1997), "Structural identification using VARMA models from noisy dynamic response under unknown random excitation", *Proceedings of International Workshop on Damage Assessment Using Advanced Signal Processing Procedures DAMAS 97*, Sheffield, UK, June, pp. 419-429.
- Fan, W. and Qiao, P. (2011), "Vibration-based damage identification methods: a review and comparative study", *Struct. Health Monitor.*, **10**(1), 83-111. <https://doi.org/10.1177/1475921710365419>
- Farrar, C.R. and Worden, K. (2007), "An introduction to structural health monitoring", *Philosophical Transactions of the Royal Society A, Mathematical, Physical and Engineering Sciences*, **365**(1851), 303-315. <https://doi.org/10.1098/rsta.2006.1928>
- Farrar, C.R. and Worden, K. (2013), *Structural Health Monitoring: A Machine Learning Perspective*, John Wiley & Sons, Chichester, UK.
- Figueiredo, E., Park, G., Figueiras, J., Farrar, C.R. and Worden, K. (2009), "Structural Health Monitoring Algorithm Comparisons Using Standard Datasets", Report LA-14393; Los Alamos National Laboratory, Los Alamos, NM, USA.
- Goi, Y. and Kim C.W. (2017), "Damage detection of a truss bridge utilizing a damage indicator from multivariate autoregressive model", *J. Civil Struct. Health Monitor.*, **7**, 153-162. <https://doi.org/10.1007/s13349-017-0222-y>
- Guidorzi, R. (2003), *Multivariable System Identification. From Observations to Models*, Bononia University Press, Bologna, Italy.
- Guidorzi, R., Losito, M. and Muratori, T. (1982), "The range error test in the structural identification of linear multivariable systems", *IEEE Transact. Automatic Control*, **27**(5), 1044-1054. <https://doi.org/10.1109/TAC.1982.1103068>
- Guidorzi, R., Diversi, R., Vincenzi, L., Mazzotti, C. and Simioli, V. (2014), "Structural monitoring of a tower by means of MEMS-based sensing and enhanced autoregressive models", *Eur. J. Control*, **20**(1), 4-13. <https://doi.org/10.1016/j.ejcon.2013.06.004>
- Heyns, P.S. (1997), "Structural damage assessment using response-only measurements", *Proceedings of International Workshop on Damage Assessment Using Advanced Signal Processing Procedures DAMAS 97*, Sheffield, UK, June, pp. 213-223.
- Ljung, L. (1987), *System Identification, Theory for the User*, Prentice-Hall, Inc, Englewood Cliffs, NJ, USA.
- Loh, C.H., Chan, C.K., Chen, S.F. and Huang, S.K. (2016), "Vibration-based damage assessment of steel structure using global and local response measurements", *Earthq. Eng. Struct. Dyn.*, **45**, 699-718. <https://doi.org/10.1002/eqe.2680>
- Mahalanobis, P.C. (1936), "On the generalized distance in statistics", *Proceedings of the National Institute of Sciences of India*, **2**(1), 49-55.
- Mosavi, A.A., Dickey, D., Seracino, R. and Rizkalla, S. (2012), "Identifying damage locations under ambient vibrations utilizing vector autoregressive models and Mahalanobis distances", *Mech. Syst. Signal Process.*, **26**, 254-267. <https://doi.org/10.1016/j.ymsp.2011.06.009>
- Nair, K.K., Kiremidjian, A.S. and Law, K.H. (2006), "Time series-based damage detection and localization algorithm with application to the ASCE benchmark structure", *J. Sound Vib.*, **291**, 349-368. <https://doi.org/10.1016/j.jsv.2005.06.016>
- Roy, K., Bhattacharya, B. and Ray-Chaudhuri, S. (2015), "ARX model-based damage sensitive features for structural damage localization using output-only measurements", *J. Sound Vib.*, **349**, 99-122. <https://doi.org/10.1016/j.jsv.2015.03.038>
- Schwarz, G.E. (1978), "Estimating the dimension of a model", *Annals Statist.*, **6**(2), 461-464. <https://doi.org/10.1214/aos/1176344136>
- Simani, S., Fantuzzi, C. and Patton, R.J. (2003), *Model-based*

*Fault Diagnosis in Dynamic Systems Using Identification Techniques*, Springer-Verlag London.

- Sohn, H., Farrar, C.R., Hemez, F.M., Shunk, D.D., Stinemates, D.W., Nadler, B.R. and Czarnecki, J.J. (2004), "A review of structural health monitoring literature: 1996–2001", Report LA-13976-MS; Los Alamos National Laboratory, Los Alamos, NM, USA.
- Wang, Z. and Ong, K.C.G. (2008), "Autoregressive coefficients based Hotelling's  $T^2$  control chart for structural health monitoring", *Comput. Struct.*, **86**, 1918-1935.  
<https://doi.org/10.1016/j.compstruc.2008.02.007>
- Worden, K., Manson, G. and Fieller, N.R.J. (2000), "Damage detection using outlier analysis", *J. Sound Vib.*, **229**(3), 647-667. <https://doi.org/10.1006/jsvi.1999.2514>